JACS
JOURNAL OF THE AMERICAN CHEMICAL SOCIETY

Article

pubs.acs.org/JACS

Huge Enhancement in Two-Photon Photoluminescence of Au Nanoparticle Clusters Revealed by Single-Particle Spectroscopy

Zhenping Guan, Nengyue Gao, Xiao-Fang Jiang, Peiyan Yuan, Fei Han, and Qing-Hua Xu*

Department of Chemistry, National University of Singapore, 3 Science Drive 3, Singapore 117543

Supporting Information

ABSTRACT: Aggregated metal nanoparticles have been known to display significantly enhanced two-photon photoluminescence (TPPL) compared to nonaggregated nanoparticles, which could be utilized to develop platforms for two-photon sensing and imaging applications. Here we have conducted single-particle spectroscopic studies on gold (Au) nanoparticle clusters of different sizes to understand the enhancement mechanisms and explore the limit of maximum achievable enhancement. Our studies show that the TPPL intensity of Au nanoparticle clusters significantly increases from monomer to trimer. The averaged intensity of the Au nanosphere dimers and linear trimers is ~7.8×10^3 and ~7.0×10^4 times that of Au nanosphere monomers, respectively. A highest enhancement of 1.2×10^5 folds was obtained for the linear trimer. The TPPL spectra of these single Au nanosphere clusters closely resemble their corresponding scattering spectra, suggesting strong correlation between their TPPL with plasmon resonance. The scattering spectra of dimers and linear trimers displayed $\cos^2$ dependence on the detection polarization, while their TPPL displayed $\cos^4$ dependence on the excitation polarization, which are very similar to Au nanorods. These results suggest that two-photon excitation of dimer and linear trimer is strongly coupled to their longitudinal plasmon resonance modes. These studies help to provide insight on fundamental understanding of the enhancement mechanisms as well as development of biomedical and photonic applications.

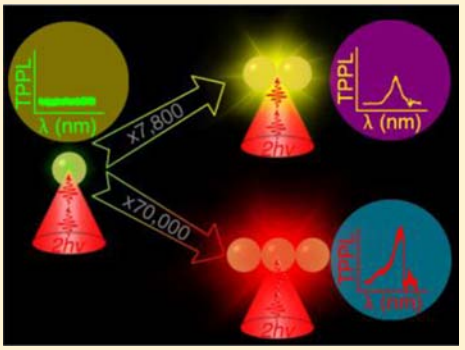

1. INTRODUCTION

Noble metal nanoparticles have been known to display many unique optical properties including surface plasmon resonance (SPR).[1] The SPR frequency can be tuned by controlling the particle size, shape, refractive index, and the interparticle plasmon coupling.[2−5] Plasmon coupling arises when metal nanoparticles come to close proximity, resulting in red-shifted SPR band and dramatically enhanced local electric field within the gap of coupled nanoparticles.[6] The giant local field enhancement would result in significantly enhanced optical responses including surface enhanced Raman scattering (SERS), second harmonic generation (SHG), metal-enhanced fluorescence, and two-photon photoluminescence (TPPL).[7−12] Nonlinear optical responses, such as TPPL, are particularly sensitive to plasmon resonance due to their quadratic dependence on the incident intensity.

Metal nanoparticles of spherical shapes typically display weak TPPL because of their relatively small two-photon absorption cross section and low emission quantum yield, while anisotropic Au NRs have been known to display strong TPPL owing to lightening rod effect.[13] Our recent studies showed that aggregation of Au and Ag nanoparticles resulted in significantly enhanced TPPL with enhancement factor of up to 100 times.[11,14−16] As many biologically important species can induce aggregation of metal nanoparticles, this phenomenon could be utilized to develop various platforms for two-photon sensing and imaging applications.[15,16] Two-photon excitation-based applications are appealing for various biological applications owing to their unique advantages, such as deep penetration into biological tissues and three-dimensional confined excitation, which allow in vivo applications.[17−19]

It is important to understand the fundamental mechanisms of aggregation-induced TPPL enhancement and explore the maximum achievable enhancement. As metal nanoparticle aggregates consist of nanoparticle clusters of different sizes, the observed enhancement is an averaged effect of these different clusters. It is thus essential to investigate their TPPL properties from the single-particle level. Most of the previous studies on TPPL of coupled metal nanostructures involved nanofabrication using electron lithography.[10,20−22] One key limitation of this method is difficulty in obtaining small-particle separation, resulting in greatly reduced field enhancement factors.[23] Single-nanoparticle spectroscopy has been widely employed to elucidate the optical properties of nanoparticles by correlating the optical responses with their well-defined structures and morphologies.[24−27] Here in this work we investigated the scattering and TPPL spectra of Au nanosphere (NS) monomers, dimers, and trimers on the single-particle level. Our studies show that the TPPL intensity of Au nanoparticle clusters increase significantly from monomer to trimer. The averaged intensity of the Au nanosphere dimers

Received: January 12, 2013
Published: April 22, 2013

   dx.doi.org/10.1021/ja400364f | J. Am. Chem. Soc. 2013, 135, 7272−7277

and linear trimers is ~7.8 × 10^3 and 7.0 × 10^4 times that of the Au nanosphere monomers, respectively. A highest enhancement of 1.2 × 10^5 folds was obtained for the linear trimer. The detection polarization dependence of the scattering spectra and excitation polarization dependence of TPPL spectra of these single Au nanosphere clusters have been performed to understand the enhancement mechanisms, which are found to closely resemble those of Au nanorods. These studies are important for fundamental understanding of enhancement mechanisms as well as development of various biomedical and photonic applications.

2. EXPERIMENTAL SECTION

2.1. Sample Preparation. Citrate-capped Au NSs with diameter of 90 nm were prepared by using a previously reported method.[28] The pH of the particle solution was first adjusted to 2.3 by using HCl before 50 μM of cysteine was added to induce the coupling of Au NSs. The resultant solution was diluted by 10 times before drop-casting onto a precleaned and marked ITO substrate. The mark allows for later pattern matching in the SEM and dark-field images to identify dimers and trimers. The sample was subsequently dried at 50 °C in an oven followed by ultrasonication for 1 min in double-distilled water to remove the excess cysteine molecules. The substrate was then dried under N_2 flow before use.

2.2. Instrumentation. Extinction spectra of Au NSs solutions were recorded on a SHIMADZU UV-2550 spectrophotometer. TEM images were acquired with a Philips CM10 TEM microscope at accelerating voltage of 100 kV. SEM images were taken on a JEOL JSM-6701F Field Emission SEM microscope at 5 kV.

2.3. TPPL Spectra Measurements in Solution. TPPL spectra were measured by using a Ti:sapphire oscillator (Avesta Ti-Sapphire TiF-100M) as the excitation source, which gives output of 785 nm laser pulses with pulse duration of 80 fs and repetition rate of 84.5 MHz. The laser beam was filtered through a 785/10 nm bandpass filter (Semrock LD01-785/10-25) to reduce their interference to the measured emission. The sample was excited by a tightly focused laser beam. The emission from the sample was collected at a 90° angle to the direction of the excitation beam to minimize the scattering. The emission signal was directed into a CCD (Princeton Instruments, Pixis 100B) coupled monochromator (Acton, Spectra Pro 2300i) with an optical fiber. The visible portion of the emission spectra was measured by using two 785 nm notch filters (Semrock NF03−785E-25) and one multiphoton 750 nm short pass filter (Semrock FF01−750/SP-25). The near-IR portion of the spectra was measured by using two 785 nm notch filters and one 808 nm long pass filter (Semrock LP02−808RU-25).

2.4. Single-Particle Scattering Spectra Measurements. The dark-field scattering spectra of immobilized Au NSs were measured by using a home-built dark-field slit imaging system based on an inverted Nikon Eclipse Ti optical microscope. A 100 W quartz−tungsten−halogen lamp in combination with a Nikon dark-field condenser (NA = 0.80−0.95) was employed as the light source. The scattering signal of the particles collected by a 100× NA = 0.5−1.25 (NA was set to 0.5) oil immersion objective was sent to a monochromator (Acton Spectra Pro 2150i) coupled CCD camera (Andor DR-328G-C01-SIL) to measure their spectra. The spectra were calibrated by dividing the normalized spectrum of illumination light source of our system. The polarized scattering spectra were measured by placing a sheet polarizer in the beam path before the detector.

2.5. Single-Particle TPPL Measurements. The 785 nm fs output of the Ti:sapphire oscillator was purified by the 785/10 nm laser filter and spatially expanded by a 5× beam expander to give a beam diameter of ~1 cm before entering the microscope. A wave plate was placed in the beam path to adjust the laser polarization. The beam was reflected by a 50/50 beam splitter into the objective lens (NA = 1.25) and focused onto the sample with a focal area of ~π × 380^2 nm^2. A piezo stage (PI E-710) movable in three dimensions was employed for the sample positioning and imaging scanning. The emission was collected by the same objective lens and filtered by the two 785 nm notch filters to suppress the laser scattering and one high-quality 450 nm long pass filter (Chroma) to remove the SHG signals. The photoluminescence was subsequently acquired by the spectrometer (Princeton Instruments) for spectral detection or by a high-quantum efficiency photon counting avalanche photodiode (APD) (PerkinElmer) together with PicoHarp 300 for intensity and imaging measurements. The background signals were recorded at the positions without nanoparticles and subtracted to obtain the final signals.

3. RESULTS AND DISCUSSION

3.1. Assembly of Au Nanoparticles. The prepared Au NSs are relatively uniform in size and shape with an average diameter of 90 nm (see TEM images in Figure S1). Cysteine was chosen as the molecular linker to assemble these Au nanoparticles. Cysteine is an amino acid containing a thiol group that can bind to the surface of Au nanoparticles. In the acidic environment, cysteine forms a zwitterionic structure, and the cooperative two-point electrostatic interactions induce the coupling of Au nanoparticles with a gap distance of ~1 nm.[29,30]

Figure 1 shows the extinction and TPPL spectra of Au NSs before and after addition of different amounts of cysteine. The

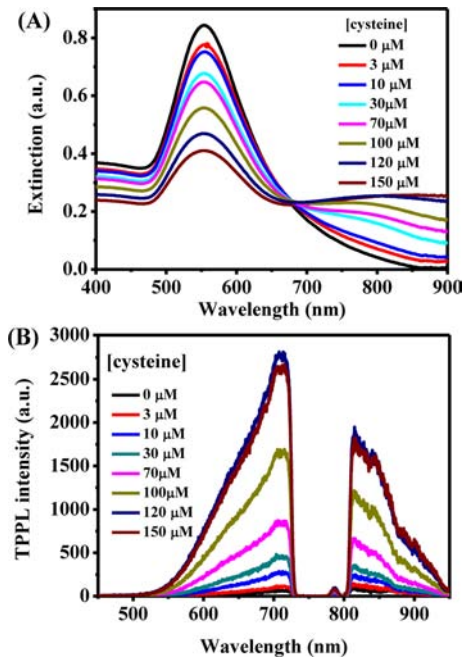

Figure 1. Extinction (A) and TPPL (B) spectra of isolated and coupled Au nanosphere solution (in the presence of different amounts of cysteine).

extinction spectrum of unaggregated Au NSs in water solution displayed a plasmon band peaking at 554 nm (Figure 1A). Upon addition of cysteine, the intensity of the original SPR band at 554 nm decreased, and a new band appeared at the longer wavelength region. This new band is a typical feature of longitudinal plasmon mode along the axis of coupled metal nanoparticles, indicating successful assembly of Au nanoparticles, which was further confirmed by their TEM images (Figure S1B).

The unaggregated Au NSs displayed very weak TPPL due to their relatively small two-photon absorption cross section and low emission quantum yield. The TPPL of Au NSs was found to be significantly enhanced upon addition of cysteine. The observed TPPL enhancement can be ascribed to the formation

dx.doi.org/10.1021/ja400364f | J. Am. Chem. Soc. 2013, 135, 7272−7277

of Au NSs assembly.[11,14−16] TPPL enhancement upon addition of different amounts of cysteine was found to follow the same trend as the change in the extinction at the excitation wavelength of 785 nm (Figure S2). A maximal enhancement of 34.5 folds was obtained in the presence of 120 μM cysteine, under which the extinction at 785 nm also reached the maximum. The two-photon excitation nature could be verified by nearly quadratic dependence of emission intensity to the excitation power densities (a slope of 1.88 was obtained from the log−log plot as shown in Figure S3).

The observed TPPL enhancement is an averaged effect of Au NS clusters of different sizes. The TEM and SEM images of the coupled Au NSs indicated the formation of Au NS clusters of different sizes including dimers, trimers, and larger clusters (Figures 2, 3, and S1). The statistical analysis based on the

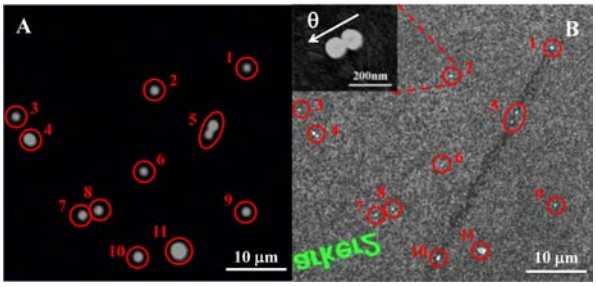

Figure 2. Dark-field scattering and SEM images of an Au nano-clusters on an ITO substrate. Inset of B is SEM image of an Au NS dimer.

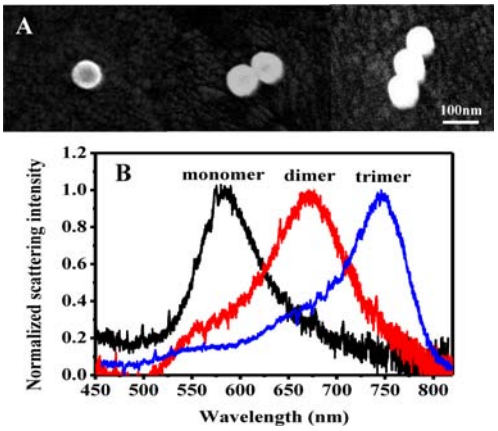

Figure 3. SEM images (A) and scattering spectra (B) of Au NS monomer, dimer, and linear trimer.

SEM images indicated that 15.4% monomer, 13.4% dimers, 16.2% trimers and a significant portion of larger clusters were formed in presence of 50 μM cysteine. The observed TPPL enhancement is an averaged effect of Au NS clusters of different sizes. To better understand the underlying enhancement mechanism, it is essential to measure the optical properties of individual Au NS clusters of different sizes on the single-particle level.

To conduct the single-particle spectroscopic studies, the coupled Au NSs solution was transferred onto an ITO substrate (see Experimental section for details). A pattern-matching method was employed to correlate the nanostructures of the coupled Au nanostructures and their spectra. The SEM and dark-field images were compared to identify the region where two images have exactly the same distributions of the particles (Figure 2). Each bright spot in the dark-field image corresponds to a nanoparticle or cluster in the SEM image. Once the correlation was established to identify different nanostructures, such as monomers, dimers, and trimers, their optical properties including scattering spectra and TPPL spectra were subsequently characterized.

3.2. Scattering Spectra of an Au NS Monomer, Dimer, and Trimer. The SEM images and scattering spectra of Au NS monomer, dimer, and linear trimer on an ITO substrate are shown in Figure 3. The scattering spectra were measured by using a slit-imaging technique.[31] The scattering spectra of the Au NS monomer displayed a SPR band with maximum at 584 nm (Figure 3B), which is red-shifted relative to that in solution owing to the effect of ITO substrate.[32] The SPR band maxima of the dimer and linear trimer were found to red-shift to 672 and 750 nm, respectively. In addition, their scattering intensities were found to significantly increase from monomer to trimer (Figure S4). These results are consistent with the previous experimental observation and plasmon hybridization model.[33−35] The red-shifted scattering spectra can be ascribed to the longitudinal mode along the assembly axis.

The scattering spectra of Au NS monomer, dimer, and linear trimer were found to display significantly different polarization dependent behaviors (Figure 4). The scattering spectra were

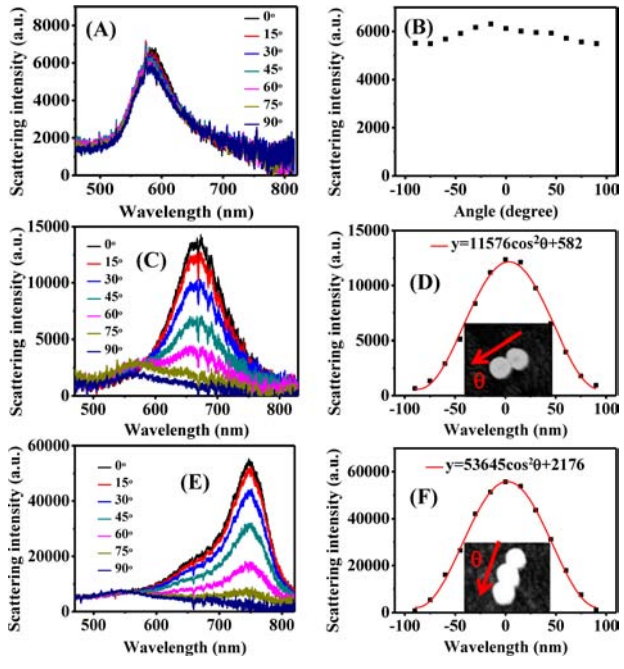

Figure 4. Polarization-dependent scattering spectra of Au NS monomer (A, B), dimer (C, D), and trimer (E, F).

detected at different polarization angles relative to the long axis of the dimer and linear trimer under illumination of unpolarized white light. The scattering spectra of the Au NS monomer displayed little polarization dependence. The subtle polarization dependence can be largely ascribed to imperfect spherical shape of the Au NS. In contrast, the scattering spectra of the Au NS dimer and linear trimer were found to strongly depend on the detection polarization. When the scattering signal was detected with polarization along the long axis (θ = 0°), the scattering spectra of the dimer and linear trimer were dominated by their longitudinal modes. However, when the scattering signal was detected with polarization perpendicular

dx.doi.org/10.1021/ja400364f | J. Am. Chem. Soc. 2013, 135, 7272−7277

to the long axis ($\theta = 90°$), the scattering intensities were much weaker, and the scattering spectra of the dimer and linear trimer were dominated by their fundamental transverse modes, which were slightly blue-shifted compared to that of the Au NS monomer. The scattering intensities of the longitudinal modes of both dimer and linear trimer gradually decreased when the polarization changed from parallel to perpendicular to the chain axis, following a $\cos^2 \theta$ function versus the polarization angles (Figures 4). The $\cos^2 \theta$ dependence is similar to that of the longitudinal mode of Au NRs,[36] confirming its origin from the longitudinal mode along the axis of the particle coupling.

The formation of new longitudinal band in dimers and linear trimers can be explained by the plasmon hybridization theory. The interparticle interactions of the coupled metal nanoparticles can be considered analogous to that of the molecular hybridization.[37] When the particles are coupled, their resonance evolves into two orthogonal modes, the red-shifted longitudinal and blue-shifted transverse modes, similar to formation of the J- and H-aggregates of the molecular excitonic coupling.[31,38]

3.3. TPPL of Au Nanoparticle Clusters. TPPL spectra of Au nanoclusters were measured by using the experimental setup illustrated in Figure S5. Femtosecond laser pulses at 785 nm with pulse duration of 80 fs and repetition rate of 84.5 MHz were used as the excitation source. The same objective lens with NA = 1.25 was employed to focus the incident laser beam and collect the emission signals as well. Two 785 nm notch filters were placed before the detector to reduce the scattering from the excitation beam. Relative higher excitation power was used, and one more high-quality 700 nm short pass filter was used to suppress the scattering from excitation laser beam for the measurement of TPPL of Au NS monomers due to its low-emission intensity. Dark-field scattering spectra were measured before and after each TPPL measurements to ensure no photothermal-induced shape transformation during the measurement processes. The two-photon excitation nature of the observed emission was confirmed by the quadratic dependence of the emission intensity on the excitation power. The log–log plot of the emission intensity of the dimer and trimer versus excitation power gives slopes of 1.94 and 2.15, which confirms that the observed photoluminescence originates from absorption of two photons (see Figure S6).[21,39]

Figure 5 shows TPPL spectra of Au NS monomer, dimer, and linear trimer with the excitation polarization parallel to the chain axis. The corresponding scattering spectra detected at polarization parallel to the chain axis are plotted in the same graph for direct comparison. It can be clearly seen that the obtained TPPL spectra of all three nanostructures closely resemble their corresponding scattering spectra. When excitation polarization is perpendicular to the chain axis, the TPPL spectra of dimers and linear trimers also closely overlap with the corresponding scattering spectra detected at the perpendicular polarization (Figure S7), although the TPPL intensities under perpendicular excitation are much weaker compared to the parallel excitation cases. These results suggest a strong relationship between the observed TPPL and the plasmon resonance bands. There are two possible mechanisms for such resemblance: plasmonic emission[21,40] and plasmon modulated emission.[41,42] These two models have been proposed by different research groups and are still under active debate. The plasmonic emission model assumes that the photoluminescence originates from radiative intraband relaxation of the surface plasmon.[21,42] The plasmon modulated emission model assumes that photoluminescence originates from the interband electron–hole recombination modulated by the surface plasmon resonance through the output emission coupling, in which surface plasmon resonance selectively amplifies the emission components with frequencies resonant with surface plasmon.[41,42]

The excitation polarization dependence of the TPPL spectra of different Au nanoparticle clusters has been further investigated in detail (Figure 6). The TPPL intensities of

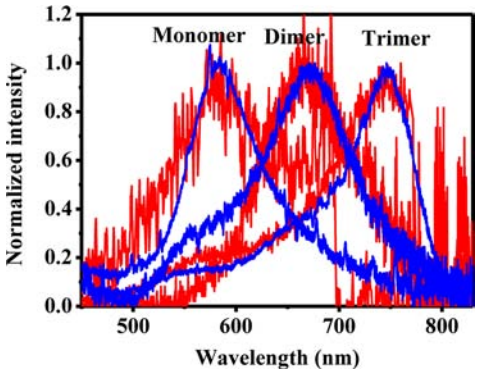

Figure 5. Normalized scattering (blue) and TPPL (red) spectra of Au NS monomer, dimer, and linear trimer.

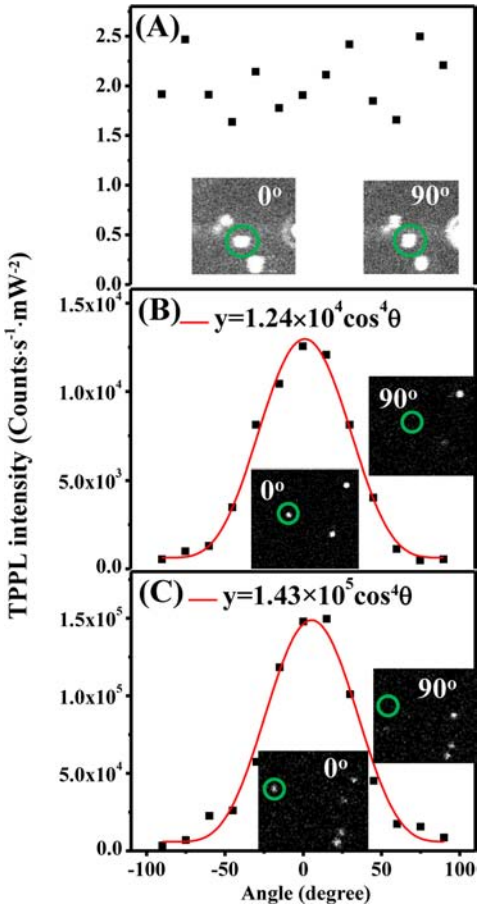

Figure 6. Excitation polarization-dependent TPPL intensities of monomer (A), dimer (B), and linear trimer (C). Insets are two-photon images of the samples with excitation polarization parallel (0°) and perpendicular (90°) to their long axis to highlight the particles being measured.

dx.doi.org/10.1021/ja400364f | J. Am. Chem. Soc. 2013, 135, 7272–7277

dimer and linear trimer show very different excitation polarization dependence from that of monomer. The integrated TPPL intensity of Au nanosphere remained nearly unchanged when the excitation polarization varied (Figure 6A). The lack of polarization dependence of TPPL in Au NS is expected due to the isotropic particle shape of the Au NS monomer. In contrast, the TPPL intensities of dimer and linear trimer display strong dependence on the excitation polarization (Figure 6B,C). The TPPL intensities of the dimer and linear trimer decrease rapidly when the polarization angle changes from 0 to 90°. Much weaker emission was observed from the dimer and linear trimer when the excitation polarization was perpendicular to the chain axis compared to that of parallel polarization. This can be directly visualized from the TPPL images shown in the inset of Figure 6B,C (more TPPL images are shown in Figure S8). The polarization angle-dependent integrated TPPL intensities can be well fit with a $\cos^4 \theta$ function. This result is similar to the previous reports on the excitation polarization-dependent TPPL in single Au nanorods,[43,44] suggesting that two-photon excitation of dimer and trimer is strongly coupled to their longitudinal plasmon resonance modes.

3.4. Relative TPPL Intensities of Three Au Nanostructures. In addition to the spectral evolution, the TPPL intensities of three Au NS cluster structures are significantly different. Figure 7 shows the TPPL intensities of 5 monomers,

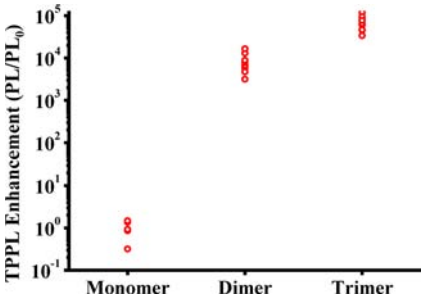

Figure 7. Relative TPPL emission intensity of Au NS monomers, dimers, and linear trimers.

10 dimers, and 10 linear trimers. The polarization was set parallel to the long axis of the dimers and trimers. To prevent undesirable damage to the nanoparticles, different excitation power intensities were used to measure the TPPL of Au NS monomers, dimers, and trimers. The relative TPPL intensities were calibrated by taking into account of the difference in excitation intensity. The scattering spectra of the particles were measured before and after each measurement to ensure no thermal reshaping of the metal nanoparticles.

By using the averaged TPPL intensity of 5 monomers as the standard, the averaged TPPL intensity of the dimers and linear trimers is $\sim 7.8 \times 10^3$ and $\sim 7.0 \times 10^4$ times that of the Au NS monomers, respectively. The variation is due to slight variation in the size of the metal nanoparticles and coupling between them. A highest enhancement of up to 1.2×10^5 fold was obtained for the linear trimer. The observed huge enhancement in TPPL intensity from monomers to dimers and linear trimers can be ascribed to a few factors. First, the longitudinal modes of dimers and linear trimers lead to increased extinction at the excitation wavelength (785 nm), which provides intermediate states to facilitate two-photon excitation processes.[11,45] This is also supported by the close correlation between the TPPL enhancement and extinction at 785 nm in the coupled nanoparticles in solution (Figure S2). On the other hand, the significant local electric field amplification at the excitation wavelength also contributes to enhanced two-photon excitation efficiency and consequently enhanced TPPL intensity. Furthermore, the plasmon coupling will cause a dynamic charge redistribution with concentrated charges at the gap region, which could further enhance the local-field intensity, especially for the resonators with sharp tip or edge-directed coupling orientation.[10,22] Plasmon resonance may also increase the quantum yield of photoluminescence,[46−50] which may also contribute to the observed TPPL enhancement. We have used ultrafast pump/probe experiments to measure the lifetime of the emitting state of unaggregated and aggregated nanoparticles in solutions. Nearly identical excited-state lifetimes were obtained for unaggregated and aggregated nanoparticles (see Figure S9), suggesting minor contribution from the change in the quantum yield of their photoluminescence, which is consistent with our previous observation in coupled Au nanocubes.[16]

It needs to be noted that the interparticle distance and coupling angle have strong influence on TPPL of these Au nanoclusters. The field enhancement in the coupled nanostructure has been known to be very sensitive to the gap distance.[51] TPPL is expected to be more sensitive to the gap distance due to its higher-order power dependence on the field enhancement. In the current study the nanoparticles were coupled by the zwitterionic interaction of two cysteine molecules, and the gap distance was fixed to be ~1 nm. The short distance ensures strong plasmon coupling and consequently significantly enhanced TPPL. We have also investigated coupling angle effect of TPPL of trimer clusters. TPPL of timers is strongly dependent on the coupling angle (see Figure S10). The trimer with coupling angle of 180° (the linear trimer) was found to display the largest TPPL intensity, which decreases rapidly as the coupling angle decreases.

4. CONCLUSIONS

By conducting single-particle scattering and TPPL studies on small Au NS clusters, we have shown that the TPPL spectra of single Au NS monomers, dimers, and linear trimers are coincident with their corresponding scattering spectra, suggesting strong correlation between their TPPL and plasmon resonance modes. The scattering and TPPL spectra of dimers and linear trimers display close resemblance to those of Au nanorods, displaying $\cos^2$ polarization-dependent scattering spectra and $\cos^4$ dependence of TPPL intensities on the excitation polarization. These results suggest that two-photon excitation of dimer and linear trimer is strongly coupled to their longitudinal plasmon resonance modes. Most importantly, the TPPL intensities of Au NS clusters increase significantly from monomers to trimers. The averaged TPPL intensity of the Au NS dimers and linear trimers is $\sim 7.8 \times 10^3$ and $\sim 7.0 \times 10^4$ times that of the monomers. A highest enhancement of up to 1.2×10^5 folds was obtained for the linear trimer. As many biologically molecules/species can induce the coupling of Au nanoparticles and result in significantly enhanced TPPL, coupling enhanced TPPL could be utilized to develop schemes for sensitive two-photon sensing and imaging applications to benefit from the unique advantages of two-photon excitation. These studies are important for both fundamental understanding of enhancement mechanisms and development of various practical applications.

■ ASSOCIATED CONTENT

Supporting Information

TEM images of isolated and aggregated Au NSs; correlation between extinction at 785 nm and TPPL enhancement of coupled Au NS solution in the presence of different amount of cysteine; excitation power dependence of the TPPL of the coupled Au NSs in solution; absolute scattering spectra of Au nanoparticle clusters; experimental setup for single-particle TPPL measurements; excitation power dependence of TPPL intensity of a dimer and a linear trimer; normalized scattering spectra detected at parallel and perpendicular polarization angles and TPPL spectra of dimer and linear trimer under parallel and perpendicular polarized laser excitation; TPPL images of three Au nanoparticle clusters with different excitation polarization angles; pump/probe measurements; SEM, scattering and TPPL spectra of Au trimers with different coupling angles. This material is available free of charge via the Internet at http://pubs.acs.org.

■ AUTHOR INFORMATION

Corresponding Author

chmxqh@nus.edu.sg.

Notes

The authors declare no competing financial interest.

■ ACKNOWLEDGMENTS

This work was supported by DSTA Singapore (project DSTA-NUS-DIRP/9010100347), the Singapore-MIT Alliance of Research and Technology (SMART) program under National Research Foundation Singapore and the Economic Development Board (SPORE, COY-15-EWI-RCFSA/N197-1). The authors would like to thank Dr. Haifeng Wang for valuable discussions and suggestions.

■ REFERENCES

(1) Ehrenreich, H.; Philipp, H. R. *Phys. Rev.* **1962**, *128*, 1622.
(2) Zhao, J.; Pinchuk, A. O.; McMahon, J. M.; Li, S.; Ausman, L. K.; Atkinson, A. L.; Schatz, G. C. *Acc. Chem. Res.* **2008**, *41*, 1710.
(3) Kelly, K. L.; Coronado, E.; Zhao, L. L.; Schatz, G. C. *J. Phys. Chem. B* **2002**, *107*, 668.
(4) Noguez, C. *J. Phys. Chem. C* **2007**, *111*, 3806.
(5) Nie, S.; Emory, S. R. *Science* **1997**, *275*, 1102.
(6) Halas, N. J.; Lal, S.; Chang, W.-S.; Link, S.; Nordlander, P. *Chem. Rev.* **2011**, *111*, 3913.
(7) Camargo, P. H. C.; Rycenga, M.; Au, L.; Xia, Y. N. *Angew. Chem., Int. Ed.* **2009**, *48*, 2180.
(8) Kinkhabwala, A.; Yu, Z.; Fan, S.; Avlasevich, Y.; Mullen, K.; Moerner, W. E. *Nat. Photonics* **2009**, *3*, 654.
(9) Jin, R.; Jureller, J. E.; Kim, H. Y.; Scherer, N. F. *J. Am. Chem. Soc.* **2005**, *127*, 12482.
(10) Ghenuche, P.; Cherukulappurath, S.; Taminiau, T. H.; van Hulst, N. F.; Quidant, R. *Phys. Rev. Lett.* **2008**, *101*, 116805.
(11) Guan, Z.; Polavarapu, L.; Xu, Q.-H. *Langmuir* **2010**, *26*, 18020.
(12) Chen, G.; Wang, Y.; Yang, M.; Xu, J.; Goh, S. J.; Pan, M.; Chen, H. *J. Am. Chem. Soc.* **2010**, *132*, 3644.
(13) Mohamed, M. B.; Volkov, V.; Link, S.; El-Sayed, M. A. *Chem. Phys. Lett.* **2000**, *317*, 517.
(14) Han, F.; Guan, Z.; Tan, T. S.; Xu, Q.-H. *ACS Appl. Mater. Interfaces* **2012**, *4*, 4746.
(15) Jiang, C.; Guan, Z.; Rachel Lim, S. Y.; Polavarapu, L.; Xu, Q.-H. *Nanoscale* **2011**, *3*, 3316.
(16) Guan, Z.; Li, S.; Cheng, P. B. S.; Zhou, N.; Gao, N.; Xu, Q.-H. *ACS Appl. Mater. Interfaces* **2012**, *4*, 5711.
(17) Tong, L.; Cobley, C. M.; Chen, J.; Xia, Y.; Cheng, J.-X. *Angew. Chem., Int. Ed.* **2010**, *49*, 3485.
(18) Jiang, Y.; Horimoto, N. N.; Imura, K.; Okamoto, H.; Matsui, K.; Shigemoto, R. *Adv. Mater.* **2009**, *21*, 2309.
(19) Polavarapu, L.; Manna, M.; Xu, Q.-H. *Nanoscale* **2011**, *3*, 429.
(20) Mühlschlegel, P.; Eisler, H.-J.; Martin, O. J. F.; Hecht, B.; Pohl, D. W. *Science* **2005**, *308*, 1607.
(21) Wissert, M. D.; Ilin, K. S.; Siegel, M.; Lemmer, U.; Eisler, H.-J. r. *Nano Lett.* **2010**, *10*, 4161.
(22) Schuck, P. J.; Fromm, D. P.; Sundaramurthy, A.; Kino, G. S.; Moerner, W. E. *Phys. Rev. Lett.* **2005**, *94*, 017402.
(23) Jain, P. K.; El-Sayed, M. A. *J. Phys. Chem. C* **2008**, *112*, 4954.
(24) Slaughter, L.; Chang, W.-S.; Link, S. *J. Phys. Chem. Lett.* **2011**, *2*, 2015.
(25) Fan, J. A.; Wu, C.; Bao, K.; Bao, J.; Bardhan, R.; Halas, N. J.; Manoharan, V. N.; Nordlander, P.; Shvets, G.; Capasso, F. *Science* **2010**, *328*, 1135.
(26) Liu, N.; Liu, H.; Zhu, S.; Giessen, H. *Nat. Photonics* **2009**, *3*, 157.
(27) Ming, T.; Zhao, L.; Chen, H.; Woo, K. C.; Wang, J.; Lin, H.-Q. *Nano Lett.* **2011**, *11*, 2296.
(28) Bastús, N. G.; Comenge, J.; Puntes, V. c. *Langmuir* **2011**, *27*, 11098.
(29) Sun, Z.; Ni, W.; Yang, Z.; Kou, X.; Li, L.; Wang, J. *Small* **2008**, *4*, 1287.
(30) Zhang, S.; Kou, X.; Yang, Z.; Shi, Q.; Stucky, G. D.; Sun, L.; Wang, J.; Yan, C. *Chem. Commun.* **2007**, 1816.
(31) Funston, A. M.; Novo, C.; Davis, T. J.; Mulvaney, P. *Nano Lett.* **2009**, *9*, 1651.
(32) Chen, H.; Sun, Z.; Ni, W.; Woo, K. C.; Lin, H.-Q.; Sun, L.; Yan, C.; Wang, J. *Small* **2009**, *5*, 2111.
(33) Barrow, S. J.; Funston, A. M.; Gómez, D. E.; Davis, T. J.; Mulvaney, P. *Nano Lett.* **2011**, *11*, 4180.
(34) Nordlander, P.; Oubre, C.; Prodan, E.; Li, K.; Stockman, M. I. *Nano Lett.* **2004**, *4*, 899.
(35) Prodan, E.; Radloff, C.; Halas, N. J.; Nordlander, P. *Science* **2003**, *302*, 419.
(36) Muskens, O. L.; Bachelier, G.; Fatti, N. D.; Vallée, F.; Brioude, A.; Jiang, X.; Pileni, M.-P. *J. Phys. Chem. C* **2008**, *112*, 8917.
(37) Guerrero-Martínez, A.; Grzelczak, M.; Liz-Marzán, L. M. *ACS Nano* **2012**, *6*, 3655.
(38) Barrow, S. J.; Funston, A. M.; Gómez, D. E.; Davis, T. J.; Mulvaney, P. *Nano Lett.* **2011**, *11*, 4180.
(39) He, G. S.; Tan, L.-S.; Zheng, Q.; Prasad, P. N. *Chem. Rev.* **2008**, *108*, 1245.
(40) Bouhelier, A.; Bachelot, R.; Lerondel, G.; Kostcheev, S.; Royer, P.; Wiederrecht, G. P. *Phys. Rev. Lett.* **2005**, *95*, 267405.
(41) Beversluis, M. R.; Bouhelier, A.; Novotny, L. *Phys. Rev. B* **2003**, *68*, 115433.
(42) Imura, K.; Nagahara, T.; Okamoto, H. *J. Am. Chem. Soc.* **2004**, *126*, 12730.
(43) Wang, H.; Huff, T. B.; Zweifel, D. A.; He, W.; Low, P. S.; Wei, A.; Cheng, J.-X. *Proc. Natl. Acad. Sci. U.S.A.* **2005**, *102*, 15752.
(44) Li, T.; Li, Q.; Xu, Y.; Chen, X.-J.; Dai, Q.-F.; Liu, H.; Lan, S.; Tie, S.; Wu, L.-J. *ACS Nano* **2012**, *6*, 1268.
(45) Biagioni, P.; Celebrano, M.; Savoini, M.; Grancini, G.; Brida, D.; Mátéfi-Tempfli, S.; Mátéfi-Tempfli, M.; Duò, L.; Hecht, B.; Cerullo, G.; Finazzi, M. *Phys. Rev. B* **2009**, *80*, 045411.
(46) Chen, H.; Ming, T.; Zhao, L.; Wang, F.; Sun, L.-D.; Wang, J.; Yan, C.-H. *Nano Today* **2010**, *5*, 494.
(47) Cheng, D.; Xu, Q.-H. *Chem. Commun.* **2007**, 248.
(48) Yuan, P.; Lee, Y. H.; Gnanasammandhan, M. K.; Guan, Z.; Zhang, Y.; Xu, Q.-H. *Nanoscale* **2012**, *4*, 5132.
(49) Ray, K.; Badugu, R.; Lakowicz, J. R. *J. Am. Chem. Soc.* **2006**, *128*, 8998.
(50) Yorulmaz, M.; Khatua, S.; Zijlstra, P.; Gaiduk, A.; Orrit, M. *Nano Lett.* **2012**, *12*, 4385.
(51) Maier, S. A.; Kik, P. G.; Atwater, H. A.; Meltzer, S.; Harel, E.; Koel, B. E.; Requicha, A. A. G. *Nat. Mater.* **2003**, *2*, 229.